HHS Public Access

Author manuscript

ACS Chem Neurosci. Author manuscript; available in PMC 2018 May 17.

Published in final edited form as:

ACS Chem Neurosci. 2018 May 16; 9(5): 1014–1026. doi:10.1021/acschemneuro.7b00428.

High-Content Microfluidic Screening Platform Used To Identify σ2R/Tmem97 Binding Ligands that Reduce Age-Dependent Neurodegeneration in *C. elegans* SC_APP Model

Sudip Monda[†,○], **Evan Hegarty**[†,○], **James J. Sahn**[‡,○], **Luisa L. Scott**[§,○], **Sertan Kutal Gökçe**[†,∥], **Chris Martin**[†,⊥], **Navid Ghorashian**[†,⊥], **Praveen Navoda Satarasinghe**[§], **Sangeetha Iyer**[§], **Wisath Sae-Lee**[#], **Timothy R. Hodges**[‡], **Jonathan T. Pierce**[*,§,#,∇], **Stephen F. Martin**[*,‡,#], and **Adela Ben-Yakar**[*,†,∥,⊥,#,∇]

[†]Department of Mechanical Engineering, The University of Texas at Austin, Austin, Texas 78712, United States

[‡]Department of Chemistry, The University of Texas at Austin, Austin, Texas 78712, United States

[§]Department of Neuroscience, The University of Texas at Austin, Austin, Texas 78712, United States

[∥]Department of Electrical and Computer Engineering, The University of Texas at Austin, Austin, Texas 78712, United States

[⊥]Department of Biomedical Engineering, The University of Texas at Austin, Austin, Texas 78712, United States

[*]Corresponding Authors: Mailing address: The University of Texas at Austin, Department of Neuroscience, College of Natural Sciences, 1 University Station, Stop C7000, Austin, TX 78712. Telephone: 512-232-4137. jonps@austin.utexas.edu., Mailing address: The University of Texas at Austin, Welch Hall 5.224, 105 E 24th Street, Stop A5300, Austin, TX 78712. Telephone: 512-471-3915. sfmartin@mail.utexas.edu., Mailing address: The University of Texas at Austin, ETC 7.132, 204 E Dean Keeton Street, Stop C2200, Austin, TX 78712. Telephone: 512-475-9280. ben-yakar@mail.utexas.edu.

[○]S.M., E.H., J.J.S., and L.L.S. contributed equally.

Orcid: Sudip Mondal: 0000-0002-5387-0064
Luisa L. Scott: 0000-0003-4518-7094
Sertan Kutal Gökçe: 0000-0001-9220-776X
Chris Martin: 0000-0002-0279-9579
Navid Ghorashian: 0000-0002-5783-4933
Jonathan T. Pierce: 0000-0002-9619-4713
Stephen F. Martin: 0000-0002-4639-0695
Adela Ben-Yakar: 0000-0003-3468-6146

Supporting Information: The Supporting Information is available free of charge on the ACS Publications website at DOI: 10.1021/acschemneur-o.7b00428.

Author Contributions: S.M. and A.B. designed the HCS platform and experiments. J.J.S., T.R.H., and S.F.M. designed and synthesized the compounds. E.H., S.M., N.G., and A.B. designed the microfluidic chip. C.M., S.M., and A.B. developed the semiautomation for image analysis GUI. S.K.G., S.M., and A.B. developed the stage automation. S.M. developed the protocols for *C. elegans* liquid culture. L.L.S., S.I., W.S.-L., P.N.S., and J.T.P. made the *C. elegans* strains, characterized neurodegeneration, and performed initial chemical screens. S.M., S.I., J.T.P., and A.B. designed the controls for the assay validation experiments. S.M., L.L.S, and A.B. designed the screening assays. S.M. performed all the screens. S.M. and A.B. prepared the HCS data analysis, representation, and statistical analysis. S.M., J.J.S., S.F.M., L.L.S., J.T.P., and A.B. wrote the manuscript.

Notes: The authors declare the following competing financial interest(s): A.B., S.M., and E.H. are co-founders of Newormics, LLC. A.B., S.M., E.H., C.M., S.K.G., and N.G. are co-inventors on patent application PCT/US2015/057624. S.F.M. and J.J.S. are co-founders of NuvoNuro, LLC. S.F.M., J.J.S., L.S., and J.T.P. are co-inventors on patent application WO2015009742A2; S.F.M., J.J.S., and T.R.H. are co-inventors on patent application WO2017070229; S.F.M. and J.J.S are also co-inventors on several other related patent applications for compounds binding to Sigma2R/Tmem97.

[#]Institute of Cell and Molecular Biology, The University of Texas at Austin, Austin, Texas 78712, United States

[▽]The Institute of Neuroscience, The University of Texas at Austin, Austin, Texas 78712, United States

Abstract

The nematode *Caenorhabditis elegans*, with tractable genetics and a well-defined nervous system, provides a unique whole-animal model system to identify novel drug targets and therapies for neurodegenerative diseases. Large-scale drug or target screens in models that recapitulate the subtle age- and cell-specific aspects of neurodegenerative diseases are limited by a technological requirement for high-throughput analysis of neuronal morphology. Recently, we developed a single-copy model of amyloid precursor protein (SC_APP) induced neurodegeneration that exhibits progressive degeneration of select cholinergic neurons. Our previous work with this model suggests that small molecule ligands of the sigma 2 receptor (σ2R), which was recently cloned and identified as transmembrane protein 97 (TMEM97), are neuroprotective. To determine structure–activity relationships for unexplored chemical space in our σ2R/Tmem97 ligand collection, we developed an in vivo high-content screening (HCS) assay to identify potential drug leads. The HCS assay uses our recently developed large-scale microfluidic immobilization chip and automated imaging platform. We discovered norbenzomorphans that reduced neurodegeneration in our *C. elegans* model, including two compounds that demonstrated significant neuroprotective activity at multiple doses. These findings provide further evidence that σ2R/Tmem97-binding norbenzomorphans may represent a new drug class for treating neurodegenerative diseases.

Graphical abstract

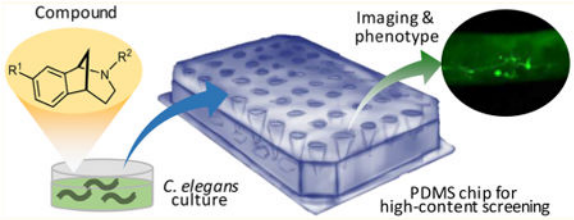

Keywords

Neurodegeneration; neurodegenerative disease models; norbenzomorphans; phenotypic screening; in vivo drug screening; C. elegans; cholinergic neurons; amyloid precursor protein; APP model; Alzheimer's disease; σ2R/TMEM97; PGRMC1; high-throughput screening; high-content screening; microfluidics; automation; high-resolution microscopy; image analysis; neuronal phenotyping

Introduction

Continuous advancements in *Caenorhabditis elegans* neurodegenerative disease models[1,2] are paving the way for high-throughput screening of collections of small molecules at the

whole organism level. Early *C. elegans* models expressed disease-related genes ectopically in muscle or at high levels in neurons causing large-scale neuromuscular dysfunction.[3] Behavioral phenotypic screening in these models has yielded important discoveries.[4,5] However, many human neurodegenerative disorders display a more subtle pattern of degeneration for specific classes of neurons.[6] Thus, next generation *C. elegans* models of neurodegeneration typically express human disease-related genes in a neuronal pattern that results in more subtle neurodegenerative phenotypes.[7] Toward this end, we recently developed a model of neurodegeneration in *C. elegans* by inserting a single-copy of the wild-type human amyloid precursor protein *APP* gene (SC_APP) into the worm genome that is expressed in all neurons.[8] Starting in adulthood, SC_APP model worms show moderate, progressive neurodegeneration of the VC4 and 5 cholinergic neurons.[8] Using this next generation model, we can screen for compounds that restrict the progress of degeneration.

The sigma 2 receptor (σ2R), which we recently cloned and identified as transmembrane protein 97 (TMEM97),[9] is distributed in the central nervous system (CNS) as well as peripheral tissues,[10] where it is involved in cell proliferation, regulation of cytosolic calcium, and cholesterol trafficking and homeostasis.[11,12] σ2R/TMEM97 has long been associated with cancer,[13,14] and it is increasingly being implicated in cellular processes relevant to a variety of CNS disorders,[10,15] including Alzheimer's disease (AD),[8,16–18] schizophrenia,[10] anxiety, pain,[19] and Niemann-Pick disease.[12]

We recently discovered that several substituted norbenzomorphans that bind with high affinity and selectivity to σ2R/Tmem97 exhibited significant neuroprotective activity in our SC_APP *C. elegans* model.[8] One of these compounds was subsequently shown to enhance cognitive performance in a transgenic APP mouse model, highlighting the predictive nature of this worm model.[8] Notably, norbenzomorphans had previously been used in only a few in vivo studies.[20,21] The discovery that neurodegenerative conditions might be mitigated via σ2R/Tmem97 modulation inspired us to create larger sets of drug-like norbenzomorphans as novel ligands for σ2R/Tmem97.[22,23] However, our ability to evaluate these compounds as neuroprotective agents in the SC_APP model was limited by the laborious nature of manually inspecting neuron health.

The lack of strong behavioral phenotypes and the restricted pattern of neurodegeneration in the SC_APP model necessitates the analysis of subtle changes in cellular morphology in order to screen for neuroprotection. The current high-throughput screening (HTS) platforms for *C. elegans*, such as plate readers,[24] lack the ability to provide the high-resolution and sensitivity required to analyze such subtle phenotypes at high speeds. In recent years, microfluidics has enabled higher resolution imaging,[25–33] some of which can be coupled with automation.[32–38] However, these microfluidic chips also lack the ability to screen at high-speeds because they can only image animals from a single population, and the requirement of significant preparation time hinders throughput.[39] Recently, we developed a large-scale microfluidic chip with ~4000 parallel immobilization channels for the analysis of 96 different populations of a poly glutamine *C. elegans* disease model.[40] Using this platform, we could evaluate the efficacy of 1000 United States Food and Drug Administration (FDA)-approved drugs in reducing the protein aggregation across the entire animal body by collecting and analyzing high-resolution data at high speeds. This platform

now provides the ability to perform in vivo high-content screening (HCS) at the speed and cost of in vitro cell based assays.

Herein, we present the high-content phenotypic screening of a set of norbenzomorphans that bind to σ2R/Tmem97 with double and triple-digit nanomolar affinity. σ2R/Tmem97 ligands had been shown to modulate neuronal degeneration at a single concentration in a *C. elegans* model of age-related neurodegeneration,[8] so we sought to identify compounds that exert dose-dependent neuroprotection utilizing our microfluidic chip-based HCS platform. The unique design of our large-scale microfluidic chip enables the immobilization of the animals in their optically favorable orientation at predetermined locations, so the neuron health can be easily assessed by evaluating fluorescently labeled cholinergic neurons at high speeds. This study identified two substituted norbenzomorphans that significantly reduce degeneration in the SC_APP animal model. These findings provide further evidence that this drug class represents a new therapeutic approach for treating neurodegenerative diseases.

Results

Age-Dependent Degeneration of Cholinergic Neurons in *C. elegans* SC_APP Model

C. elegans is a proven platform for elucidating disease pathways, in part because of the ease with which genetic modifications can induce the expression of human disease-causing proteins. The *C. elegans* model of neurodegeneration that we recently developed expresses a copy of wild-type human APP engineered into chromosome II, referred to herein as SC_APP.[8] APP has been extensively studied because one of its cleaved peptide products, amyloid β, forms the hallmark plaques of AD. Mutations in the APP gene are associated with altered risk of developing AD, and the copy number of wild-type *APP* appears to associate with disease likelihood.[41] In our SC_APP *C. elegans* model, pan-neuronal expression of human *APP* induces age-dependent degeneration.[8] Six VC-class cholinergic neurons appear vulnerable to SC_APP-induced degeneration. Of all six VC neurons, VC4 and 5 in SC_APP animals are the most susceptible to degeneration, as indicated by the shrinkage or elimination of the fluorescent cell body and the neuronal processes (Figure 1a). These VC4 and 5 neurons show a substantial increase in neurodegeneration with age (Figure 1b), well correlated with the morphological changes in the phase-contrast images of the neurons,[8] indicating that the SC_APP strain is useful for screening compounds for protection against age- and APP-related neurodegeneration. Both day 3 (D3) and day 5 (D5) adult age animals display statistically higher degeneration percentages compared to WT ($P < 0.001$; Figure 1b).

Subtle Phenotypes Preclude a Behavioral Readout for Large-Scale Screens of Treatment Efficacy

Behavioral assays are commonly used to find treatments that alter neurological outcomes in *C. elegans*. The VC4 and 5 neurons, along with the HSN neurons, uv1 neuroendocrine cells, and the vm1 and vm2 vulva muscles, comprise the egg laying neuromuscular circuitry. Calcium transients in VC neurons, particularly VC4 and 5, are temporally associated with egg laying events.[42] Thus, we analyzed egg laying behavior to determine if behavioral differences could be used to screen for neuroprotective treatments. Consistent with a recent

report of silencing VC neuron activity that did not alter the number of unlaid eggs, [43] we found no difference in the average number of unlaid eggs on D1 or D3 of adulthood for SC_APP and WT worms (Figure 2a). We did find a broadening in the distribution of the number of unlaid eggs (Figure 2b), which could relate to differences in VC4 and 5 functions between SC_APP and WT animals.[42,44] The percent of animals with 20 or more eggs was significantly higher in SC_APP (28 ± 11%, corresponding to mean ±95% confidence interval) versus WT (8 ± 5%) animals (Fisher's exact test: $P < 0.01$). However, this phenotypic difference was too subtle to support a high-throughput screen based on behavior.

Next, we examined whether locomotor changes could serve as a readout for VC4 and 5 neurodegeneration because previous work indicates VC neurons modulate locomotion.[42] We first tested whether VC neuron ablation by cell-specific expression of human Casp1 (ICE) impaired swimming. As similar results were found for head bend rate and swim speed, only swim speed is reported. Using an alternate WT background with the VC4 and 5 neurons brightly labeled by *Ptph-1:GFP* expression, we found that VC-specific expression of ICE starting at L4 led to very dim, small VC4 and 5 neurons on D1 of adulthood (10/10 worms). Despite an overall age-related decline in swim speed ($P < 0.001$) consistent with previous findings,[45] additional deficits in swimming were seen on both D1 and D5 of adulthood when the VC neurons were genetically ablated ($P < 0.001$, Figure 2c). The SC_APP and corresponding WT background strains also showed an age-related decline in swim speed ($P < 0.001$, Figure 2d). However, the swim speed, head bend rate and the kinematics of swimming in older adults (D5) was similar between SC_APP and WT animals, likely because VC neuron degeneration was not extensive enough to produce additional measurable deficits. Interestingly, swim speed was significantly faster in SC_APP animals than WT for D1 adults.

As a control to test if the subtle difference in D1 swimming could arise due to the trivial reason that the SC_APP transgene interfered with the development of the VC neurons prior to neurodegeneration, we ensured that VC4 and 5 fully differentiated into adult neurons in the SC_APP strain prior to morphological signs of degeneration.[8] To do so, we verified that a transcriptional reporter for terminal cholinergic fate (*Punc-4:mCherry*) was expressed in VC4 and 5 neurons in L4 and D1 adult SC_APP animals (Supplementary Figure 1).[46,47]

Together, these findings show that SC_APP animals largely maintain behavioral integrity in egg laying and swimming relative to age-matched WT controls. The limited expression of behavioral phenotypes in this SC_APP is consistent with a restricted pattern of neurodegeneration. However, a lack of strong behavioral phenotypes at an early stage necessitates the analysis of fluorescence-based subtle changes in VC4 and 5 cellular morphology in order to screen for neuroprotective treatments. Since D3 animals are easier to handle than the more fragile D5 animals, we used D3 SC_APP animals for screening the health of VC4 and 5 neurons using our microfluidic screening chip.

Neuroprotective Properties of σ2R/Tmem97-Binding Norbenzomorphans in SC_APP Model

Accumulating evidence suggests σ2R/Tmem97 ligands may be useful for treating neurodegenerative diseases. σ2R/Tmem97-targeted compounds exhibit neuroprotective properties in vitro[17] as well as neuroprotective and cognition enhancing properties in vivo.

[8,16] We have recently shown that small molecules that bind to σ2R/Tmem97 can be neuroprotective in our *C. elegans* SC_APP model, and one of these improves cognitive function in a transgenic APP mouse model.[8] Here, we begin to further assess the hypothesis that σ2R/Tmem97 binding ligands might be promising leads to treat neurodegenerative diseases. To explore the effects of σ2R/Tmem97 ligands comprising the norbenzomorphan scaffold, we prepared a collection of novel, drug-like analogues. We used a modular synthetic platform that enables facile access to a broad array of norbenzomorphan analogues.[18,48–50] These new compounds were screened at the Psychoactive Drug Screening Program (PDSP), University of North Carolina, Chapel Hill,[51] and binding affinities at rodent σRs were scored (Table 1).[22,23] Two of these compounds, SAS-0132 and JVW-1009, were previously tested at a single dose in the SC_APP animals using a manual imaging method.[8] To identify additional compounds, compare the efficacy across methodologies, further develop structure-activity relationships, and begin to probe target pathway information, we selected seven more compounds having double and triple-digit nanomolar binding affinities for σ2R/Tmem97. Siramesine was also selected because it is a known σ2R/Tmem97 agonist.[52] We then used our HCS microfluidic imaging platform as discussed in the next section to assess the effects of multiple concentrations of these 10 compounds.

High-Resolution and High-Speed Microfluidic Imaging Platform for High-Content Screening (HCS) of C. elegans

We recently developed a microfluidic immobilization chip that enabled a large-scale screening of polyglutamine-induced aggregation model in *C. elegans*, requiring high-resolution detection and analysis of 1–5 μm size aggregates distributed in three-dimensions in a fully automated manner.[40] However, detection of weak fluorescence signals from a degenerating neuron present in our SC_APP model not only requires capturing high-resolution images but also immobilization of the animals in their optically favorable lateral orientations. Such weak signals together with the increasing body fluorescence in adults, deteriorate the signal to background ratio significantly as the animal age, making the image analysis a very difficult task if the images are not captured with good contrast. To enable imaging conditions with a good signal to background ratio and high contrast, we designed a unique tapered 3D channel with nearly a constant aspect ratio which facilitates maintaining the lateral orientation of the animals as they are pushed into the channels by an on/off pressure cycle. The channels' unique design thus allows placing the VC4 and 5 neurons along the channel side walls with a greater optical accessibility for the high-resolution imaging assays. This configuration was crucial in capturing the subtle changes in fluorescence signal of the faded intensity of degenerating neurons.

The large-scale, polydimethylsiloxane (PDMS) microfluidic immobilization chip[40] can immobilize ~4000 animals from 96 populations growing in liquid culture (LC) and treated with different compounds (Figure 3a). Underneath each well, there are 40 parallel channels that can immobilize the animals in predetermined locations (Figure 3b). An automated image acquisition system collects fluorescence images of immobilized animals with 1 μm resolution. The neuronal images located along the ventral cord are captured, with an optimized stage control for precise focusing on the laterally oriented animals, from 12 different heights separated by 5 μm steps to resolve the neurons in the best focus plane and

in 4 different fields of view (FOVs) per well to capture all 40 parallel trapping channels (Figure 3c). A total of 4608 images (96 wells × 4 FOVs/well × 12 images/FOV) are acquired from the whole 96-well chip in less than 12 min.

The imaging platform was accompanied by a new graphic user interference (GUI) for semiautomated analysis of tens of thousands of images quickly since manual image analysis of subtle phenotypical changes precludes large-scale screens (Figure 3d). The specialized GUI simplified the data handling of the large number of images while substantially reducing the time required for their analysis. The GUI automatically uploads the images, finds the channels with a trapped animal, and displays the best focal plane for one animal at a time to the user for neuronal phenotyping for VC4 and 5. The VC4 and 5 neurons are scored as 1) “normal” (bright fluorescence intensity and an oval shaped cell morphology), 2) “degenerated” (diminished or no intensity), or 3) “do not score” (the animal is not in the orientation for the neuron to be visible). The program also contains additional scoring options on several body features (Supplementary Figure 2). It saves all phenotypical scores for each animal in a multidimensional array. Using this GUI, we can analyze all 4608 images collected from a single chip for the neuronal health of the trapped animals in approximately 8 h. This semiautomated analysis successfully reduced the data processing time by at least an order of magnitude compared to when all the automated steps of the GUI performed manually.

All ~4000 D3 adult animals from 96 different populations can be immobilized within ~3 min with 95% of the trapping channels successfully filled with animals and with more than 90% of them optimally oriented in their lateral positions for scoring. Implementing and integrating the semiautomated image analysis algorithm with the microfluidic immobilization chip have enabled, for the first time, a large-scale and high-content study of a neurodegeneration model in *C. elegans* with the subtle phenotypes.

Drug Screening Assay Validation Using the HCS Platform for *C. elegans* SC_APP Model

We first needed to determine the minimum number of animals to be analyzed in order to provide a statistically meaningful screen for hit identification. The most commonly used parameter to determine this number is the screening window coefficient, defined as $Z' - \text{factor}, = 1 - 3\left(\frac{\sigma_1 + \sigma_2}{|\mu_1 - \mu_2|}\right)$, which should be in the range of $0.5 \leq Z'$-factor < 1 to provide the highest quality data.[53] This parameter utilizes the average (μ) and standard deviation (σ) to identify the dynamic range of the assay signal and the data variation associated with the signal measurements to represent the noise band ($\mu \pm 3\sigma$). Hits are identified as those compounds whose signals are shifted more than the separation band between the sample and the control. To determine the Z'-factor in our screen, we measured the average degeneration percentages (μ) and the standard deviations (σ) of both healthy (WT) and degenerating (SC_APP) animals loaded in the 96-well chip using the pattern shown in Figure 4a. The phenotypical scores registered in the GUI are exported as a heat-map and a scattered plot (Figure 4b,c). The results showed that the assay could provide a satisfactory screening window coefficient Z'-factor ≥ 0.5 when pooling together data from two or three wells (Figure 4d,e).

To validate the sensitivity of our assay and provide a dose—response, we tested three chemical compounds relevant to human neurodegenerative diseases: bexarotene (BEX); SB399885 (SB); and P7C3 at four different concentrations (Figure 5). Bexarotene is a retinoid X receptor agonist that was reported to enhance the clearance of soluble Aβ protein and improve behavioral deficits in mouse models.[54] While bexarotene has also been shown to reduce network hyper-excitability[55] and reverse apoE4-induced cognitive and neuronal impairments,[56] its favorable effects on Aβ could not be replicated by others.[57,58] Compound SB399885 is a 5-HT_6 receptor antagonist and has been shown to improve memory and reduce anxiety in mice.[59] P7C3 was initially selected for the ability to restrict death among adult-born neurons in mice.[60] Later, P7C3 and its derivatives were found to protect against neurodegeneration[61] and axonal degeneration in mouse and *C. elegans* models,[62] likely by activating the rate-limiting enzyme in the salvage of nicotinamide adenine dinucleotide.[63] Our assay included both WT and SC_APP model animals treated with each of these compounds at four different concentrations in LC (Figure 5a). We loaded each population of animals into three separate wells of the 96-well chip to have a sufficient number of animals for phenotyping, thereby increasing the confidence level for comparison, as determined above, to provide $Z' > 0.5$.

The results for all three compounds showed dose-dependent neuroprotection of the VC4 and 5 neurons from degeneration in the SC_APP model (Figure 5b,c). In control experiments, neither the addition of 0.5% DMSO (vehicle) nor drug treatment of WT animals affected the degeneration percentages statistically. Both bexarotene and SB399885 had strong dose dependencies, with the highest efficacy in protecting against neurodegeneration at 20 μM in the SC_APP model (Figure 5d,e). On the other hand, P7C3 shows neuroprotection at the 0.2 μM level with reduced levels at higher dosages.[64] In addition to their higher efficacy, higher dosages of bexarotene and SB399885 show low variability in terms of degeneration percentages between three different wells when compared to the P7C3-treated animals (Figure 5c). Other phenotypes, such as axonal degeneration and body autofluorescence, could also be extracted from the images using the GUI to collect subcellular phenotypes and evaluate animal health exposed to a specific compound, respectively (Supplementary Figure 3). These experiments validate both the ability of our SC_APP model as a tool to identify the efficacy of known compounds, as well as the effectiveness of our new HCS platform to screen these compounds against subtle age-related degeneration of specific cholinergic neurons with unprecedented speed.

Screening Norbenzomorphans for Neuroprotective Activity in the SC_APP Model

To evaluate the dose-dependent neuroprotective properties of the selected set of nine norbenzomorphans (Table 1), we utilized our HCS platform and the SC_APP model (Figure 6). As a control, we tested siramesine, which is a well-characterized and commercially available σ2R/Tmem97 ligand (K_i = 0.12 nM).[52] The results show that siramesine and the σ2R/Tmem97 binding ligands 7, DKR-1005, and 9 increase neurodegeneration after a dosing threshold is exceeded despite an initial decrease at lower dosages (U-shaped dose–response).[64] Conversely, the three norbenzomorphans SAS-0132, 2, and JVW-1009, which are approximately equipotent in this assay, reduce neurodegeneration relative to the vehicle treated SC_APP group. Notably, the σ2R/Tmem97 ligands SFM-1500 and SAS-1121

exhibit pronounced neuroprotective effects, decreasing neurodegeneration in SC_APP mutants to WT control levels. The ligand 3 also significantly reduces neurodegeneration with ascending dosing through 2 μM, after which neuron loss begins to increase (U-shaped dose–response).

Previously, we found that the degeneration of VC4 and 5 in the SC_APP model is dependent on *vem-1*,[8] the *C. elegans* ortholog of the progesterone receptor membrane component 1 (PGRMC1).[65] Consistent with other work,[16,17] we also found that SAS-0132 and JVW-1009 reduced neurodegeneration through a pathway dependent upon PGRMC1.[8] To further understand the mode of action of the compounds tested herein, we studied the effect of two different dosages of all compounds on the degeneration rates in a SC_APP strain expressing a *vem-1*/PGRMC1 null mutant allele (Supplementary Figure 4). In agreement with our previous findings, genetically eliminating *vem-1*/PGRMC1 function in the SC_APP model reduced neurodegeneration to near WT levels. None of the ligands further reduced basal neurodegeneration in this strain, indicating that they confer neuroprotection via a PGRMC1-mediated pathway. Collectively, our results clearly demonstrate that our microfluidics screening platform can be exploited to evaluate the neuroprotective properties of small molecules in a dose-dependent fashion, thereby identifying potential candidates for further evaluation.

■ Discussion

Most large-scale drug screening efforts using *C. elegans* disease models have been limited to gross behavioral or cellular phenotypes. Although these studies have yielded valuable information, a better way to discover relevant therapeutic compounds entails observing subtle cellular phenotypic changes in novel *C. elegans* disease models that better model disease progression in humans. We recently developed a *C. elegans* model of APP-induced neurodegeneration, which we used to find two novel neuroprotective compounds with high affinity for σ2R/Tmem97. Here we further characterized our SC_APP model, finding a limited expression of behavioral phenotypes consistent with a restricted pattern of neurodegeneration. To enable a larger scale screen for neuroprotective treatments, we developed a platform capable of the high-throughput analysis[40] of the subtle changes in VC4 and 5 cellular morphology seen in the SC_APP model. Our new in vivo HCS platform for imaging multiple *C. elegans* populations allowed us to screen unexplored chemical space of our σ2R/Tmem97 ligand collection. Using this platform, we discovered norbenzomorphans that demonstrate significant neuroprotective activity in our *C. elegans* model.

The technical challenge presented by our SC_APP model was the need for high-throughput detection of a decay in the VC neuronal fluorescence and/or an alteration in cell geometries in the presence of a sizable fluorescence background. To meet this need, we have developed a microfluidic imaging platform that solves a number of the technological limitations in terms of control of animal orientation, imaging speed and resolution, and compatibility with commercial liquid handling systems.[40] High speeds are possible because our large-scale microfluidic chip includes 96-wells, each equipped with individual parallel traps, and can quickly immobilize all 4000 animals in predetermined locations and in their optically favorable orientation. The automated system can then acquire high-resolution images of all

animals within 12 min (in addition to ~3 min for immobilization). Our HCS microfluidics platform using the SC_APP *C. elegans* assay provided a quality factor of Z'-factor ≥ 0.5 when data from two wells/populations were combined to reduce the standard deviation. Importantly, the assay confirmed the efficacy of clinically relevant compounds such as bexarotene and SB399885, both of which protected the cholinergic neurons of the SC_APP model.

Recent studies indicate that dietary restriction, exercise and FUdR treatment increase longevity and/or decrease the toxicity of aggregating proteins in *C. elegans*.[66–69] As such, modifications to growth conditions accommodating the HCS platform could impact the level of neurodegeneration. Previously, we assayed neurodegeneration in SC_APP worms cultured on bacteria-seeded plates.[8] By comparison, worms grown in LC in the current study may be expected to decrease dietary intake[69–71] and increase "exercise" by swimming,[66,72] potentially conferring neuroprotection. FUdR, used in both assays to eliminate the need for daily picking or filtering, would be expected to reduce neurodegeneration.[67,68,73–75] Consistent with these expectations, we found a slightly lower but statistically insignificant (except for the D1 adult SC_APP animals) rate of neurodegeneration for SC_APP worms grown in the liquid than on plates (Supplementary Table 1). The putative neuroprotective effect of culturing worms in liquid medium appeared to benefit the adult SC_APP strain more than it prevented basal degeneration in our WT control. This may indicate that the effects of dietary restriction and swimming are especially beneficial when adult worms are challenged with the expression of a potentially toxic protein like APP.

Overexpression of wild-type APP appears to cause Alzheimer's disease in people with Down syndrome and in rare individuals without Down syndrome who carry an extra copy of APP.[41,76] A well-studied cause of APP-related toxicity is its natural cleavage product, Aβ. Recently, a genetic manipulation that restricted Aβ toxicity in yeast was found to restrict neurodegeneration in a worm model expressing human Aβ as well primary rat cortical neurons exposed to Aβ[7]. Because C. *elegans* lacks an obvious ortholog for β-secretase APP is not likely to be processed into Aβ in our model. Instead, our SC_APP model might better recapitulate aspects of neurodegeneration caused by portions of the APP other than Aβ. Other cleavage products of APP likely found in the worm, such as the C99 intracellular peptide, can also cause neuronal dysfunction in mouse models resembling human Alzheimer's disease.[77] We have found that neuroprotection in our C *elegans* SC_APP model predicts cognitive improvements in a transgenic mouse model that overexpresses APP.[8] These improvements in cognition occurred without a reduction in Aβ burden, perhaps indicating a non-Aβ; related mechanism.

To identify new σ2R/Tmem97 receptor ligands with high binding affinities and determine their effects on neurodegeneration in our SC_APP *C. elegans* model, we selected nine compounds and tested them using our HCS platform. All these compounds were tested for a range of doses, a task that would have been prohibitively time-consuming if performed manually. Notably, the two σ2R/Tmem97 ligands, SFM-1500 and SAS-1121, elicited a significant reduction in neurodegeneration in the SC_APP model at low concentrations (0.2–2.0 μM). This result is encouraging in light of a recent study reporting that drug uptake by *C. elegans* is comparable to that of mice, especially when they are treated in a LC environment.

[78] Moreover, our recent study with SAS-0132 has demonstrated an improvement in cognitive performance in transgenic AD mice.[8] Finally, the dose-dependent variations observed even within this small compound collection show that our microfluidic screening technology is an excellent platform for assessing structure–activity-relationships.

Our HCS platform also supports target validation studies. The σ2R was recently cloned and identified as TMEM97 in mammals,[9] but we have not yet verified the *C. elegans* TMEM97 ortholog. The most likely candidate is Y38H6C.16, which shows conservation of a key asparagine residue for σ2R/TMEM97 ligand binding.[79] Nonetheless, our previous findings in the SC_APP model[8] and work in other neurodegeneration models[16,17] indicates that the neuroprotective effects of σ2R/Tmem97 ligands can be eliminated in the absence of PGRMC1. A potential requirement for PGRMC1 activity provided a way to probe target validation using our HCS platform. We found that none of the σ2R/Tmem97 ligands tested herein reduced basal neurodegeneration in a SC_APP strain expressing a null mutant allele of the worm PGRMC1 ortholog.[65] This finding suggests that these compounds act through a conserved PGRMC1-mediated pathway. It will be interesting to determine in the future whether PGRMC1 is part of a universal pathway generally required for σ2R/Tmem97 compound activity, or a requirement more specific to neuroprotective effects.

In summary, our transgenic single-copy human APP *C. elegans* model was used to identify norbenzomorphans with neuroprotective activity. Using our HCS platform, we have successfully screened multiple drugs in different doses to identify hits using a *C. elegans* disease model. Notably, SFM-1500 and SAS-1121 exhibit significant neuroprotection at all four applied concentrations. Because the related norbenzomorphan, SAS-0132, is efficacious both in *C. elegans* and a transgenic APP mouse model,[8] this *C. elegans* neurodegeneration model may have important predictive value for candidate identification. Thus, this screen not only determined neuroprotective efficacy in *C. elegans* but also selected compounds for further use in mammalian studies. Indeed, candidate compounds are being evaluated in higher animals for their effects in a variety of neurodegenerative conditions. We surmise that norbenzomorphans identified in this and future applications of this powerful HCS assay may be promising leads as therapeutics for neurodegenerative conditions.[22] More generally, we expect this HCS microfluidic technology to be broadly applicable to test small molecules in *C. elegans* models that capture the subtle cellular phenotypes characteristic of the human disease. The ability to screen whole-animal models at unprecedented speeds and with high resolution will facilitate the identification and translation of promising preclinical candidates.

■ Methods

Strains

C. elegans were grown and maintained on nematode growth medium (NGM) agar plates with bacteria at 20 °C according to the standard method.[80] We used the following *C. elegans* strains for the neurodegeneration assays in this work: LX959 *vsIs13 [lin-11::pes-10::GFP + lin-15(+)] IV lin-15B(n765) X*, JPS67 *vxSi38 [Prab-3::huAPP695::unc-54UTR, Cb unc-119(+)] II unc-119(ed3) III vsIs13 IV*, JPS449 *vxSi38 II; unc119(ed3) III; vsIs13 IV; lin15b(n765), vem-1(gk220) X*, and JPS607 *vxSi38 II; unc-119(ed3) III; vxIs13 IV;*

lin15b(n765) vem-1(ok1058) X. LX959, JPS67, JPS449, and JPS607 expressed GFP in all six VC neurons and were considered as WT and SC_APP models, *vem-1*/PGRMC1 null, and *vem-1*/PGRMC1 null (allele 2), respectively. LX959 and JPS67 were used for the behavioral assays along with JPS617 *vxIs591[ptph-1::GFP::unc-54UTR]*, JPS768 *vxEx768[VC-specific(lin-11::pes-10)::ICE::unc-54UTR, pmyo-2::mCher-ry::unc-54UTR]; vxIs591[ptph-1::GFP:: unc-54UTR]*, and JPS769 *vxEx769[VC-specific(lin-11::pes-10) ::ICE:unc-54UTR, pmyo-2::mCherry:: unc-54UTR]; vxIs591[ptph-1::GFP::unc-54UTR]*. The VC neuron-specific promoter used to make JPS768 and JPS769 was kindly provided by Michael Koelle, Yale University.

Transgenesis

Transgenic animals with a single copy of pan-neuronal *huAPP695* full length (kindly provided by Chris Li, City College of New York) were generated through the MOSSCI technique as previously described.[81] Briefly, we used Gateway technology (Invitrogen) to construct a vector with the *huAPP695* (cDNA) gene driven by the pan-neuronal promoter (*Prab-3*) and an *unc-54* UTR adjacent to the *Cb_unc-119(+)* positive selection marker. Transgenes were flanked by Mos1 transposon insertion sites complementary to a specific region on the second (ttTi5605) chromosome. *unc-119* mutant animals with specific Mos1 insertions sites were then injected with DNA. Selection of mobile, nonfluorescent progeny led us to identify single-copy insertion animals. Full insertion of APP was confirmed by PCR.

Chemicals

All chemicals for *C. elegans* maintenance were bought from Fisher Scientific and Sigma-Aldrich. Drug compounds P7C3 (2 M Biotec), bexarotene (Sigma-Aldrich, lot no: 024M4723 V), and SB 399885 hydrochloride (Tocris, lot no: 2A/148640) were dissolved in DMSO (Sigma-Aldrich, lot no: RNBD6062) at 100 mM and used at four different concentrations in the worm culture as mentioned in the text. 5-Fluoro-2-deoxyuridine (FUdR, Sigma-Aldrich, lot no: SLBL9184 V) was dissolved in water.

σ2R/Tmem97 Ligands and Their Binding Assays

A collection of compounds were generated using a modular synthetic platform to afford a diverse array of substituted heterocycles (Supplementary Note 1) that was screened against σ1R, σ2R, and other CNS targets.[22,23] Briefly, the compounds were dissolved in 100% DMSO prior to the receptor binding assays, which were performed by the Psychoactive Drug Screening Program (PDSP) at Chapel Hill, North Carolina. The assay protocol book can be accessed free of charge at: http://pdspdb.unc.edu/pdspWeb/content/PDSP%20Protocols%20II%202013-03-28.pdf. Briefly, σ2R/Tmem97 was sourced from rat PC12 cells. σ2R/Tmem97 ligand binding affinity was determined through competition binding assays using the radioligand [^{3}H]-ditolylguanidine in the presence of (+)-pentazocine to block σ1R binding sites. The radioactivity in the presence of the test compound is calculated with the following equation and expressed as a percent inhibition: % inhibition = (sample CPM – nonspecific CPM)/(total CPM – nonspecific CPM) × 100, where CPM stands for counts per minute. To determine secondary binding data, CPM/well are pooled and fitted to

a three-parameter logistic function for competition binding in Prism v 5.0 to determine IC_{50} values, which are converted to K_i according to the Cheng-Prusoff equation.

Unlaid Eggs

To count the number of unlaid eggs in the uterus, individual age-matched worms were singled out in wells with 5% bleach. Eggs were counted after the worms split open.

Swim Speed

Age-matched worms were cleaned of bacteria, submerged in NGM liquid, and recorded following a 2 min acclimation period at 2 frames/s with a FLEA digital camera (Point Gray, Richmond, BC, Canada). The distance that the worms swam during 1 min was measured using a semiautomated procedure in ImagePro Plus (Media Cybernetics, Rockville, MD) to objectively calculate the overall speed of individual worms.

Confocal Imaging

Worms were mounted on 2% agarose pads, immobilized with 30 mM sodium azide and imaged with a Zeiss laser-scanning microscope (LSM710) using Zen (black edition) acquisition software (Carl Zeiss, Germany). GFP fluorescence and phase contrast images were collected using a 488 nm laser and mCherry fluorescence was collected using a 561 nm laser. Using a 63× water immersion objective and a 0.9 mm pinhole, neurons were imaged in three dimensions taking slices every 0.8 mm through the *z*-axis.

Large-Scale Liquid Culture of *C. elegans*

To culture *C. elegans* populations in large quantities and facilitate efficient loading of the microfluidic chip without clogging the narrow trapping channels, we used a new liquid culturing (LC) protocol that we recently developed for *C. elegans* in S medium with HB101 bacteria.[40] Animals were first synchronized as previously mentioned. Briefly, gravid animals growing on NGM plates were bleached and eggs were allowed to hatch in the buffer at 20 °C in a 360° rotor for 24 h. Age synchronized L1s were filtered and plated in 24 wells with approximately 300 animals per well. The culture medium of 1 mL with HB101 bacteria was added to all wells and shaken on a horizontal shaker at 80 rpm for 48 h and at 20 °C to achieve homogeneous bacterial density. The fresh bacterial culture of 500 μL and 200 μM sterility drug (FUdR) was added to every well. Appropriate drug compounds were added at late L4 larval stages in designated wells to maintain the same concentration. The plates were incubated for 72 h at 80 rpm. The wells were filtered and loaded into three different wells on a primed chip for high-speed and high-resolution imaging.

Large-Scale 96-Well Microfluidic Chip Fabrication

We fabricated the microfluidic chips using three-layer photolithography and single-layer soft-lithography techniques as described earlier.[40] Briefly, a three-layer mold was fabricated on a 6 in. silicon wafer. The SU8 mold was treated with tridecafluoro-1,1,2,2-tetrahydrooctyl-1-trichlorosilane vapor (United Chemical Technologies) to avoid unwanted surface adhesion with the silicon surface. To mold a microfluidic chip, polydimethylsiloxane (PDMS, Dow Corning) was mixed in the ratio 10:1 and poured on the silanized SU8 mold.

A 96-well PCR plate placed on top of the SU8 features made the wells. The PDMS chip was cured at 70 °C for 2 h, peeled from the SU8 mold, released from the PCR plate, punched for exits (Syneo), and bonded to a 3/16-in. borosilicate glass substrate using 100 W oxygen plasma. The whole chip was finally cured at 70 °C for 6 h for complete sealing.

Chip Operation

The chip operates using a gasket system, designed to match the standard well plate dimensions. Gasket-2 has one buffer entry port and one air vent, and is held tight using screws to avoid leakage. We pipet ~80 adult worms per well. After installation of the chip within the gasket system, we open both exits (Exit1 and Exit2) while initiating a computer controlled on/off pressure cycle. The whole 96-well chip with 3840 traps can be filled with animals in approximately 4 min after which we move the stage to initiate imaging A01 well.

Automated Image Acquisition

We developed an automation LabVIEW software to control the CCD camera, the flat-top translational stage, and the 500 μm traveling range (±2 nm) piezo stage (MS2000, Applied Scientific Instrumentation) for automated imaging of all trapped animals. The imaging was performed using an Olympus IX73 microscope, equipped with a large area 15 × 15 mm^2, 4 megapixels, 7.4 × 7.4 μm^2 pixel size, 15 frames per second maximum frame rate CCD camera (MegaPlus ES4020, Princeton Instruments). The software controlled the exposure time of the camera and its synchronization with the movement of a motorized stage platform. The camera could capture 10 immobilization channels in the field of view (FOV) and the all 40 channels within a well in 4 FOVs. Taking into account predetermined channel offsets, automated imaging algorithm can acquire 12 z-stack images from all 96 wells in less than 12 min generating ~40 GB of images that are stored as 16-bit TIFF images.

Automated Image Analysis Processes in the GUI

The GUI rapidly loads the saved image stacks at specific locations of the chip from a given screen. To identify each worm immobilized inside the microfluidic channels, the program adds all the stacks into a single image to increase the contrast between the neurons and surrounding areas, applies a Gaussian low-pass filter ($\sigma = 1.0$) to attenuate high-frequency features, projects the summed image to the axis perpendicular to the length of the worm, and searches for peaks (Figure 3d). To predict the plane of best focus for the VC4 and 5 neurons, the program crops each channel with trapped animal, removes foreign particles such as eggs and debris, by thresholding and size-filtering, and then finds the plane with the brightest pixel within a region around the center of the animal, where the neurons are located. The whole animal at the focal plane is finally displayed to the user for scoring along with a pseudo movie including a set of ±5 z-stack images around the plane of best focus. Every animal is scored for VC4 and 5 health and whole-body phenotypes (Supplementary Figure 2). The data of phenotypical scores are saved in the multidimensional array to be extracted for statistical analysis.

Statistical Analysis

We analyzed the statistical significance of the scores using two-tailed Fisher's exact test. Where measurement was repeated in multiple batches, mean values were calculated to represent in the graph. The quality of the screen was quantified by calculating the Z′-factor.[53] In percent degeneration representation for the WT and SC_APP animals, we represented the error bars as the 95% confidence interval (CI) assuming a normal distribution.

Supplementary Material

Refer to Web version on PubMed Central for supplementary material.

Acknowledgments

We thank Aubri Kottek, Dr. Ryan Doonan, and Travis Jarrell for their assistance with animal maintenance and initial work with liquid culture. LX959 strain was provided by the CGC, which is funded by NIH Office of Research Infrastructure Programs (P40 OD010440). We are grateful to Dr. Richard Pederson (Materia, Inc.) for catalyst support. We thank Dr. Steve McKnight from The University of Texas at Southwestern Medical Center for providing P7C3 for our assay validation experiments. We also thank Ricky Garza for technical assistance. Screening of small molecules against a panel of CNS targets was provided by the National Institute of Mental Health's Psychoactive Drug Screening Program, Contract # HHSN-271-2013-00017-C (NIMH PDSP). The NIMH PDSP is directed by Bryan L. Roth MD, PhD at the University of North Carolina at Chapel Hill and Project Officer Jamie Driscoll at NIMH, Bethesda, MD.

Funding: The authors would like to thank the National Institutes of Health for the financial support with the NIH Director's Transformative Award from the National Institute on Aging (NIA R01 AG041135), NIH grants from the National Institute of Neurological Disorders and Stroke (NINDS R21 NS067340 and NINDS R21 NS058646), from the National Institute on Aging (NIA R01 RF1AG057355), and a training grant from the National Institute of Biomedical Imaging and Bioengineering (NIBIB T32 EB007507), Lumind Research Down Syndrome, and The Robert A. Welch Foundation (F-0652).

References

1. Teschendorf D, Link CD. What have worm models told us about the mechanisms of neuronal dysfunction in human neurodegenerative diseases? Mol Neurodegener. 2009; 4:38. [PubMed: 19785750]
2. Dimitriadi M, Hart AC. Neurodegenerative disorders: insights from the nematode *Caenorhabditis elegans*. Neuro-biol Dis. 2010; 40:4–11.
3. Link CD. *C. elegans* models of age-associated neurodegenerative diseases: lessons from transgenic worm models of Alzheimer's disease. Exp Gerontol. 2006; 41:1007–1013. [PubMed: 16930903]
4. Link CD. Expression of human beta-amyloid peptide in transgenic *Caenorhabditis elegans*. Proc Natl Acad Sci U S A. 1995; 92:9368–9372. [PubMed: 7568134]
5. Kraemer BC, Zhang B, Leverenz JB, Thomas JH, Trojanowski JQ, Schellenberg GD. Neurodegeneration and defective neurotransmission in a *Caenorhabditis elegans* model of tauopathy. Proc Natl Acad Sci U S A. 2003; 100:9980–9985. [PubMed: 12872001]
6. Yankner BA, Lu T, Loerch P. The aging brain. Annu Rev Pathol: Mech Dis. 2008; 3:41–66.
7. Treusch S, Hamamichi S, Goodman JL, Matlack KES, Chung CY, Baru V, Shulman JM, Parrado A, Bevis BJ, Valastyan JS, Han H, Lindhagen-Persson M, Reiman EM, Evans DA, Bennett DA, Olofsson A, DeJager PL, Tanzi RE, Caldwell KA, Caldwell GA, Lindquist S. Functional links between Aβ toxicity, endocytic trafficking, and Alzheimer's disease risk factors in yeast. Science. 2011; 334:1241–1245. [PubMed: 22033521]
8. Yi B, Sahn JJ, Ardestani PM, Evans AK, Scott LL, Chan JZ, Iyer S, Crisp A, Zuniga G, Pierce JT, Martin SF, Shamloo M. Small molecule modulator of sigma 2 receptor is neuroprotective and reduces cognitive deficits and neuroinflammation in experimental models of Alzheimer's disease. J Neurochem. 2017; 140:561–575. [PubMed: 27926996]

9. Alon A, Schmidt HR, Wood MD, Sahn JJ, Martin SF, Kruse AC. Identification of the gene that codes for the sigma2 receptor. Proc Natl Acad Sci U S A. 2017; 114:7160–7165. [PubMed: 28559337]
10. Guo L, Zhen X. Sigma-2 receptor ligands:neurobiological effects. Curr Med Chem. 2015; 22:989–1003. [PubMed: 25620095]
11. Bartz F, Kern L, Erz D, Zhu M, Gilbert D, Meinhof T, Wirkner U, Erfle H, Muckenthaler M, Pepperkok R, Runz H. Identification of cholesterol-regulating genes by targeted RNAi screening. Cell Metab. 2009; 10:63–75. [PubMed: 19583955]
12. Ebrahimi-Fakhari D, Wahlster L, Bartz F, Werenbeck-Ueding J, Praggastis M, Zhang J, Joggerst-Thomalla B, Theiss S, Grimm D, Ory DS, Runz H. Reduction of TMEM97 increases NPC1 protein levels and restores cholesterol trafficking in Niemann-pick type C1 disease cells. Hum Mol Genet. 2016; 25:3588–3599. [PubMed: 27378690]
13. Mach RH, Zeng C, Hawkins WG. The sigma2 receptor: a novel protein for the imaging and treatment of cancer. J Med Chem. 2013; 56:7137–7160. [PubMed: 23734634]
14. Huang YS, Lu HL, Zhang LJ, Wu Z. Sigma-2 receptor ligands and their perspectives in cancer diagnosis and therapy. Med Res Rev. 2014; 34:532–566. [PubMed: 23922215]
15. Matsumoto, RR., Bowen, WD., Su, TP. Sigma Receptors: Chemistry, Cell Biology, and Clinical Implications. Springer; New York: 2007.
16. Izzo NJ, Staniszewski A, To L, Fa M, Teich AF, Saeed F, Wostein H, Walko T 3rd, Vaswani A, Wardius M, Syed Z, Ravenscroft J, Mozzoni K, Silky C, Rehak C, Yurko R, Finn P, Look G, Rishton G, Safferstein H, Miller M, Johanson C, Stopa E, Windisch M, HutterPaier B, Shamloo M, Arancio O, LeVine H 3rd, Catalano SM. Alzheimer's therapeutics targeting amyloid beta 1–42 oligomers I: Abeta 42 oligomer binding to specific neuronal receptors is displaced by drug candidates that improve cognitive deficits. PLoS One. 2014; 9:e111898. [PubMed: 25390368]
17. Izzo NJ, Xu J, Zeng C, Kirk MJ, Mozzoni K, Silky C, Rehak C, Yurko R, Look G, Rishton G, Safferstein H, Cruchaga C, Goate A, Cahill MA, Arancio O, Mach RH, Craven R, Head E, LeVine H 3rd, Spires-Jones TL, Catalano SM. Alzheimer's therapeutics targeting amyloid beta 1–42 oligomers II: Sigma-2/PGRMC1 receptors mediate Abeta 42 oligomer binding and synaptotoxicity. PLoS One. 2014; 9:e111899. [PubMed: 25390692]
18. Martin SF, Sahn JJ, Scott L, Pierce-Shimomura JT. Compounds and methods for treating cancer, neurological disorders, ethanol withdrawal, anxiety, depression, and neuropathic pain. 2015 Jan. 22:2015. WO2015009742 A2.
19. Sahn JJ, Mejia GL, Ray PR, Martin SF, Price TJ. Sigma 2 receptor/Tmem97 agonists produce long lasting antineuropathic pain effects in mice. ACS Chem Neurosci. 2017; 8:1801–1811. [PubMed: 28644012]
20. Jacobson AE, Mokotoff M. Azabicyclo chemistry. I. Synthesis of 1,5-methano-7-methoxy-2,3,4,5-tetrahydro-1H-2-benza-zepines. B-norbenzomorphans. J Med Chem. 1970; 13:7–9. [PubMed: 5412120]
21. Chen YL, Liston D, Nielsen J, Chapin D, Dunaiskis A, Hedberg K, Ives J, Johnson J Jr, Jones S. Syntheses and anticholinesterase activity of tetrahydrobenzazepine carbamates. J Med Chem. 1994; 37:1996–2000. [PubMed: 8027982]
22. Sahn JJ, Hodges TR, Chan JZ, Martin SF. Norbenzomorphan framework as a novel scaffold for generating sigma2 receptor/PGRMC1 subtype-selective ligands. Chem Med Chem. 2016; 11:556–561. [PubMed: 26915462]
23. Sahn JJ, Hodges TR, Chan JZ, Martin SF. Norbenzomorphan scaffold: chemical tool for modulating sigma receptor-subtype selectivity. ACS Med Chem Lett. 2017; 8:455–460. [PubMed: 28435536]
24. Gosai SJ, Kwak JH, Luke CJ, Long OS, King DE, Kovatch KJ, Johnston PA, Shun TY, Lazo JS, Perlmutter DH, Silverman GA, Pak SC. Automated high-content live animal drug screening using *C. elegans* expressing the aggregation prone serpin alpha1-antitrypsin Z. PLoS One. 2010; 5:e15460. [PubMed: 21103396]
25. Chronis N, Zimmer M, Bargmann CI. Microfluidics for *in vivo* imaging of neuronal and behavioral activity in *Caenorhabditis elegans*. Nat Methods. 2007; 4:727–731. [PubMed: 17704783]

26. Guo SX, Bourgeois F, Chokshi T, Durr NJ, Hilliard MA, Chronis N, Ben-Yakar A. Femtosecond laser nanoaxotomy lab-on-a-chip for *in vivo* nerve regeneration studies. Nat Methods. 2008; 5:531–533. [PubMed: 18408725]
27. Zeng F, Rohde CB, Yanik MF. Sub-cellular precision on-chip small-animal immobilization, multi-photon imaging and femtosecond-laser manipulation. Lab Chip. 2008; 8:653–656. [PubMed: 18432331]
28. Krajniak J, Lu H. Long-term high-resolution imaging and culture of *C. elegans* in chip-gel hybrid microfluidic device for developmental studies. Lab Chip. 2010; 10:1862–1868. [PubMed: 20461264]
29. Samara C, Rohde CB, Gilleland CL, Norton S, Haggarty SJ, Yanik MF. Large-scale *in vivo* femtosecond laser neurosurgery screen reveals small-molecule enhancer of regeneration. Proc Natl Acad Sci U S A. 2010; 107:18342–18347. [PubMed: 20937901]
30. Mondal S, Ahlawat S, Rau K, Venkataraman V, Koushika SP. Imaging *in vivo* neuronal transport in genetic model organisms using microfluidic devices. Traffic. 2011; 12:372–385. [PubMed: 21199219]
31. Caceres, IdC, Valmas, N., Hilliard, MA., Lu, H. Laterally orienting *C. elegans* using geometry at microscale for high-throughput visual screens in neurodegeneration and neuronal development studies. PLoS One. 2012; 7:e35037. [PubMed: 22536350]
32. Crane MM, Stirman JN, Ou CY, Kurshan PT, Rehg JM, Shen K, Lu H. Autonomous screening of *C. elegans* identifies genes implicated in synaptogenesis. Nat bMethods. 2012; 9:977–980.
33. Lee H, Crane MM, Zhang Y, Lu H. Quantitative screening of genes regulating tryptophan hydroxylase transcription in *Caenorhabditis elegans* using microfluidics and an adaptive algorithm. Integr Biol. 2013; 5:372–380.
34. Chung K, Crane MM, Lu H. Automated on-chip rapid microscopy, phenotyping and sorting of *C. elegans*. Nat Methods. 2008; 5:637–643. [PubMed: 18568029]
35. Chung K, Lu H. Automated high-throughput cell microsurgery on-chip. Lab Chip. 2009; 9:2764–2766. [PubMed: 19967110]
36. Gökçe SK, Guo SX, Ghorashian N, Everett WN, Jarrell T, Kottek A, Bovik AC, Ben-Yakar A. A fully automated microfluidic femtosecond laser axotomy platform for nerve regeneration studies in *C. elegans*. PLoS One. 2014; 9:e113917. [PubMed: 25470130]
37. Gokce SK, Hegarty EM, Mondal S, Zhao P, Ghorashian N, Hilliard MA, Ben-Yakar A. A multi-trap microfluidic chip enabling longitudinal studies of nerve regeneration in *Caenorhabditis elegans*. Sci Rep. 2017; 7:9837. [PubMed: 28852096]
38. Ghorashian N, Gökçe SK, Guo SX, Everett WN, Ben-Yakar A. An automated microfluidic multiplexer for fast delivery of *C. elegans* populations from multiwells. PLoS One. 2013; 8:e74480. [PubMed: 24069313]
39. Ben-Yakar A, Chronis N, Lu H. Microfluidics for the analysis of behavior, nerve regeneration, and neural cell biology in *C. elegans*. Curr Opin Neurobiol. 2009; 19:561–567. [PubMed: 19896831]
40. Mondal S, Hegarty E, Martin C, Gokce SK, Ghorashian N, Ben-Yakar A. Large-scale microfluidics providing high-resolution and high-throughput screening of *Caenorhabditis elegans* poly-glutamine aggregation model. Nat Commun. 2016; 7:13023. [PubMed: 27725672]
41. Zigman WB, Lott IT. Alzheimer's disease in Down syndrome: neurobiology and risk. Ment Retard Dev Disabil Res Rev. 2007; 13:237–246. [PubMed: 17910085]
42. Collins KM, Bode A, Fernandez RW, Tanis JE, Brewer JC, Creamer MS, Koelle MR. Activity of the *C. elegans* egg-laying behavior circuit is controlled by competing activation and feedback inhibition. eLife. 2016; 5:e21126. [PubMed: 27849154]
43. Kopchock, R., Arvelo, E., Garcia, P., Coffey, W., Collins, K. 21st International C elegans Meeting. UCLA; Los Angeles, CA: 2017. Dissecting the function of acetylcholine in the *C. elegans* egg-laying behavior circuit; p. 952C
44. Bany IA, Dong MQ, Koelle MR. Genetic and cellular basis for acetylcholine inhibition of *Caenorhabditis elegans* egg-laying behavior. J Neurosci. 2003; 23:8060–8069. [PubMed: 12954868]

45. Schreiber MA, Pierce-Shimomura JT, Chan S, Parry D, McIntire SL. Manipulation of behavioral decline in *Caenorhabditis elegans* with the Rag GTPase raga-1. PLoS Genet. 2010; 6:e1000972. [PubMed: 20523893]

46. Zheng C, Karimzadegan S, Chiang V, Chalfie M. Histone methylation restrains the expression of subtype-specific genes during terminal neuronal differentiation in *Caenorhabditis elegans*. PLoS Genet. 2013; 9:e1004017. [PubMed: 24348272]

47. Lickteig KM, Duerr JS, Frisby DL, Hall DH, Rand JB, Miller DM 3rd. Regulation of neurotransmitter vesicles by the homeodomain protein UNC-4 and its transcriptional corepressor UNC-37/groucho in *Caenorhabditis elegans* cholinergic motor neurons. J Neurosci. 2001; 21:2001–2014. [PubMed: 11245684]

48. Sahn JJ, Martin SF. Expedient synthesis of norbenzomorphan library via multicomponent assembly process coupled with ring-closing reactions. ACS Comb Sci. 2012; 14:496–502. [PubMed: 22857149]

49. Martin SF. Strategies for the Synthesis of Alkaloids and Novel Nitrogen Heterocycles. Adv Heterocycl Chem. 2013; 110:73–117.

50. Sahn JJ, Granger BA, Martin SF. Evolution of a strategy for preparing bioactive small molecules by sequential multicomponent assembly processes, cyclizations, and diversification. Org Biomol Chem. 2014; 12:7659–7672. [PubMed: 25135846]

51. Besnard J, Ruda GF, Setola V, Abecassis K, Rodriguiz RM, Huang XP, Norval S, Sassano MF, Shin AI, Webster LA, Simeons FR, Stojanovski L, Prat A, Seidah NG, Constam DB, Bickerton GR, Read KD, Wetsel WC, Gilbert IH, Roth BL, Hopkins AL. Automated design of ligands to polypharmacological profiles. Nature. 2012; 492:215–220. [PubMed: 23235874]

52. Perregaard J, Moltzen EK, Meier E, Sanchez C. Sigma ligands with subnanomolar affinity and preference for the sigma 2 binding site 1. 3-(omega-aminoalkyl)-1H-indoles. J Med Chem. 1995; 38:1998–2008. [PubMed: 7783131]

53. Zhang JH, Chung TD, Oldenburg KR. A simple statistical parameter for use in evaluation and validation of high throughput screening assays. J Biomol Screening. 1999; 4:67–73.

54. Cramer PE, Cirrito JR, Wesson DW, Lee CY, Karlo JC, Zinn AE, Casali BT, Restivo JL, Goebel WD, James MJ, Brunden KR, Wilson DA, Landreth GE. ApoE-directed therapeutics rapidly clear β-amyloid and reverse deficits in AD mouse models. Science. 2012; 335:1503–1506. [PubMed: 22323736]

55. Bomben V, Holth J, Reed J, Cramer P, Landreth G, Noebels J. Bexarotene reduces network excitability in models of Alzheimer's disease and epilepsy. Neurobiol Aging. 2014; 35:2091–2095. [PubMed: 24767949]

56. Boehm-Cagan A, Michaelson DM. Reversal of apoE4-driven brain pathology and behavioral deficits by bexarotene. J Neurosci. 2014; 34:7293–7301. [PubMed: 24849361]

57. Veeraraghavalu K, Zhang C, Miller S, Hefendehl JK, Rajapaksha TW, Ulrich J, Jucker M, Holtzman DM, Tanzi RE, Vassar R, Sisodia SS. Comment on “ApoE-directed therapeutics rapidly clear β-amyloid and reverse deficits in AD mouse models”. Science. 2013; 340:924.

58. Fitz NF, Cronican AA, Lefterov I, Koldamova R. Comment on “ApoE-directed therapeutics rapidly clear β-amyloid and reverse deficits in AD mouse models”. Science. 2013; 340:924.

59. Wesolowska A, Nikiforuk A. Effects of the brain-penetrant and selective 5-HT6 receptor antagonist SB-399885 in animal models of anxiety and depression. Neuropharmacology. 2007; 52:1274–1283. [PubMed: 17320917]

60. Pieper AA, Xie S, Capota E, Estill SJ, Zhong J, Long JM, Becker GL, Huntington P, Goldman SE, Shen CH, Capota M, Britt JK, Kotti T, Ure K, Brat DJ, Williams NS, MacMillan KS, Naidoo J, Melito L, Hsieh J, De Brabander J, Ready JM, McKnight SL. Discovery of a proneurogenic, neuroprotective chemical. Cell. 2010; 142:39–51. [PubMed: 20603013]

61. De Jesus-Cortes H, Xu P, Drawbridge J, Estill SJ, Huntington P, Tran S, Britt J, Tesla R, Morlock L, Naidoo J, Melito LM, Wang G, Williams NS, Ready JM, McKnight SL, Pieper AA. Neuroprotective efficacy of aminopropyl carbazoles in a mouse model of Parkinson disease. Proc Natl Acad Sci U S A. 2012; 109:17010–17015. [PubMed: 23027934]

62. Yin TC, Britt JK, De Jesus-Cortes H, Lu Y, Genova RM, Khan MZ, Voorhees JR, Shao J, Katzman AC, Huntington PJ, Wassink C, McDaniel L, Newell EA, Dutca LM, Naidoo J, Cui H, Bassuk AG,

Harper MM, McKnight SL, Ready JM, Pieper AA. P7C3 neuroprotective chemicals block axonal degeneration and preserve function after traumatic brain injury. Cell Rep. 2014; 8:1731–1740. [PubMed: 25220467]

63. Wang G, Han T, Nijhawan D, Theodoropoulos P, Naidoo J, Yadavalli S, Mirzaei H, Pieper AA, Ready JM, McKnight SL. P7C3 neuroprotective chemicals function by activating the rate-limiting enzyme in NAD salvage. Cell. 2014; 158:1324–1334. [PubMed: 25215490]
64. Calabrese EJ. Alzheimer's disease drugs: an application of the hormetic dose-response model. Crit Rev Toxicol. 2008; 38:419–451. [PubMed: 18568864]
65. Runko E, Kaprielian Z. *Caenorhabditis elegans* VEM-1, a novel membrane protein, regulates the guidance of ventral nerve cord-associated axons. J Neurosci. 2004; 24:9015–9026. [PubMed: 15483120]
66. Chuang HS, Kuo WJ, Lee CL, Chu IH, Chen CS. Exercise in an electrotactic flow chamber ameliorates age-related degeneration in *Caenorhabditis elegans*. Sci Rep. 2016; 6:28064. [PubMed: 27305857]
67. Aitlhadj L, Sturzenbaum SR. The use of FUdR can cause prolonged longevity in mutant nematodes. Mech Ageing Dev. 2010; 131:364–365. [PubMed: 20236608]
68. Feldman N, Kosolapov L, Ben-Zvi A. Fluorodeoxyuridine improves *Caenorhabditis elegans* proteostasis independent of reproduction onset. PLoS One. 2014; 9:e85964. [PubMed: 24465816]
69. Kapahi P, Kaeberlein M, Hansen M. Dietary restriction and lifespan: Lessons from invertebrate models. Ageing Res Rev. 2017; 39:3–14. [PubMed: 28007498]
70. Steinkraus KA, Smith ED, Davis C, Carr D, Pendergrass WR, Sutphin GL, Kennedy BK, Kaeberlein M. Dietary restriction suppresses proteotoxicity and enhances longevity by an hsf-1-dependent mechanism in *Caenorhabditis elegans*. Aging Cell. 2008; 7:394–404. [PubMed: 18331616]
71. Kim DK, Kim TH, Lee SJ. Mechanisms of aging-related proteinopathies in *Caenorhabditis elegans*. Exp Mol Med. 2016; 48:e263. [PubMed: 27713398]
72. Laranjeiro R, Harinath G, Burke D, Braeckman BP, Driscoll M. Single swim sessions in *C. elegans* induce key features of mammalian exercise. BMC Biol. 2017; 15:30. [PubMed: 28395669]
73. Van Raamsdonk JM, Hekimi S. FUdR causes a twofold increase in the lifespan of the mitochondrial mutant gas-1. Mech Ageing Dev. 2011; 132:519–521. [PubMed: 21893079]
74. Rooney JP, Luz AL, Gonzalez-Hunt CP, Bodhicharla R, Ryde IT, Anbalagan C, Meyer JN. Effects of 5′-fluoro-2-deoxyuridine on mitochondrial biology in *Caenorhabditis elegans*. Exp Gerontol. 2014; 56:69–76. [PubMed: 24704715]
75. Anderson EN, Corkins ME, Li JC, Singh K, Parsons S, Tucey TM, Sorkac A, Huang H, Dimitriadi M, Sinclair DA, Hart AC. *C. elegans* lifespan extension by osmotic stress requires FUdR, base excision repair, FOXO, and sirtuins. Mech Ageing Dev. 2016; 154:30–42. [PubMed: 26854551]
76. Prasher VP, Farrer MJ, Kessling AM, Fisher EM, West RJ, Barber PC, Butler AC. Molecular mapping of Alzheimer-type dementia in Down's syndrome. Ann Neurol. 1998; 43:380–383. [PubMed: 9506555]
77. LaFerla FM, Green KN, Oddo S. Intracellular amyloid-beta in Alzheimer's disease. Nat Rev Neurosci. 2007; 8:499–509. [PubMed: 17551515]
78. Zheng SQ, Ding AJ, Li GP, Wu GS, Luo HR. Drug absorption efficiency in *Caenorhbditis elegans* delivered by different methods. PLoS One. 2013; 8:e56877. [PubMed: 23451103]
79. The C. elegans Sequencing Consortium. Genome sequence of the nematode *C. elegans*: a platform for investigating biology. Science. 1998; 282:2012–2018. [PubMed: 9851916]
80. Brenner S. The genetics of *Caenorhabditis elegans*. Genetics. 1974; 77:71–94. [PubMed: 4366476]
81. Frokjaer-Jensen C, Davis MW, Hopkins CE, Newman BJ, Thummel JM, Olesen SP, Grunnet M, Jorgensen EM. Single-copy insertion of transgenes in *Caenorhabditis elegans*. Nat Genet. 2008; 40:1375–1383. [PubMed: 18953339]

Abbreviations

SC_APP single copy amyloid precursor protein

WT	wild type
σ2R	sigma 2 receptor
AD	Alzheimer's disease
Tmem97	transmembrane protein 97
PGRMC1	progesterone receptor membrane component 1
VC4 and 5	VC-class cholinergic neurons 4 and 5
LC	liquid culture
FUdR	5-Fluoro-2-deoxyuridine
DMSO	dimethyl sulfoxide
PDMS	polydimethylsiloxane
HCS	high-content screening
HTS	high-throughput screening
GUI	graphic user interface

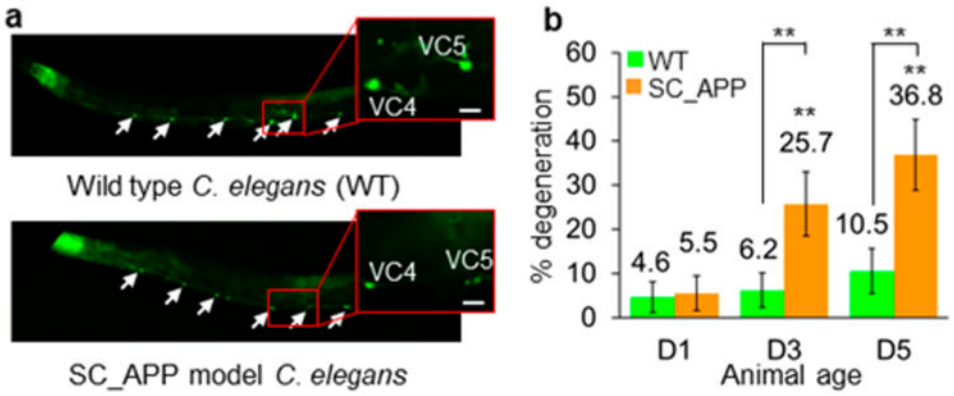

Figure 1.

Age-dependent neurodegeneration in SC_APP *C. elegans* model. (a) Fluorescence images of day 3 (D3) adult WT and SC_APP model animals. White arrows show all six VC neurons. The insets present VC4 and 5 neurons that we specifically scored for degeneration. In the bottom image, the VC4 and 5 neurons of a SC_APP animal show reduced fluorescence and contracted somata indicating degeneration. Scale bars are 10 μm. (b) Percent degeneration of VC4 and 5 neurons in WT and SC_APP model animals as a function of their age as determined by manual imaging using anesthetics on agar pads. The data represented as mean ± 95% confidence intervals. Symbols above the brackets refer to group comparisons between same-age SC_APP model and WT worms. Symbols directly above the orange bars indicate group comparisons to day 1 (D1) SC_APP model worms. $P < 0.001$ (**); $n > 100$ neurons ($n > 50$ animals).

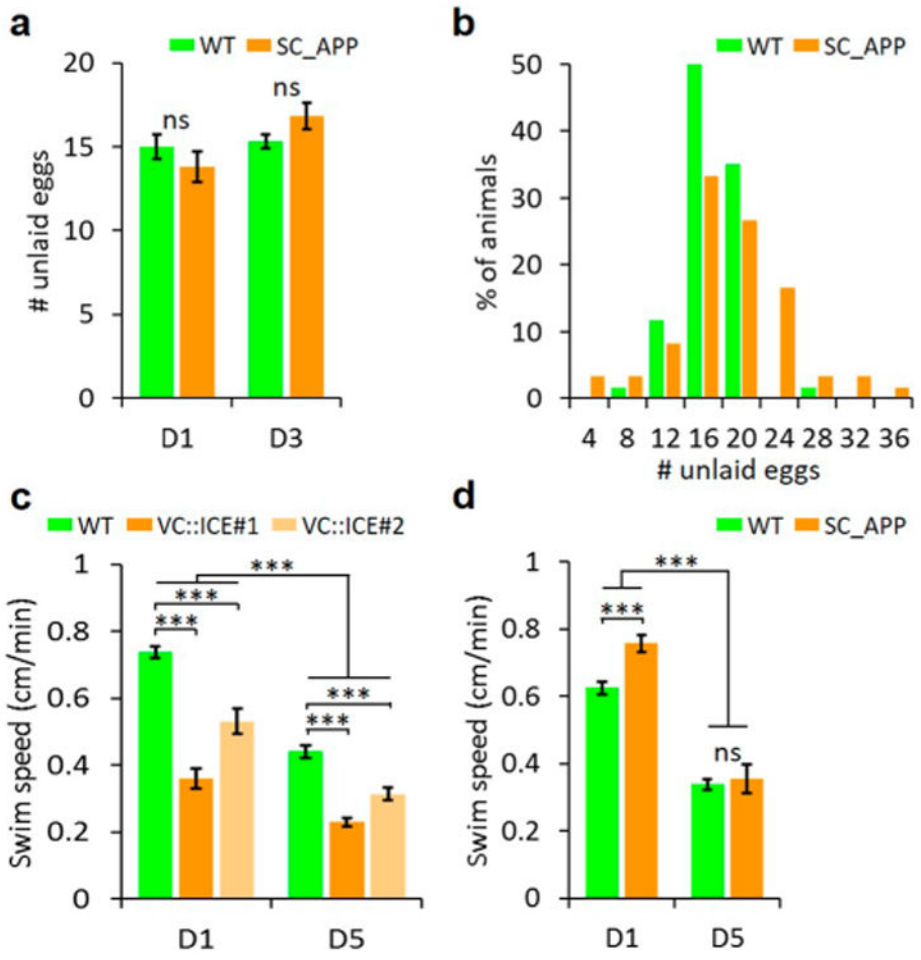

Figure 2.

Subtle behavioral phenotypes in C. elegans model with SC_APP-induced neurodegeneration. (a) Mean number of unlaid eggs ± SEM on D1 and D3 of adulthood was similar for SC_APP and WT worms (n = 61–70). (b) Distribution of the number of unlaid eggs in the same set of D3 adults as in (a) shows a broader distribution for SC_APP than WT worms (n = 63–71). The percent of worms with ≥ 20 eggs was significantly higher in SC_APP than WT worms (Fisher's exact test, $P < 0.01$). (c) Mean swim speed ± SEM on D1 and D5 of adulthood for WT and VC::ICE strains. There was an overall reduction in swim speed with age (Holm-Sidack posthoc test, $P < 0.001$, n = 50–113). Genetic ablation of VC neurons caused an additional reduction in swim speed at each age relative to WT (Holm-Sidack posthoc tests, $P < 0.001$, n = 50-113). (d) Mean swim speed ± SEM on D1 and D5 of adulthood for WT and SC_APP strains. There was an overall reduction in swim speed with age (Holm–Sidack posthoc test, $P < 0.001$, n = 46–105). SC_APP worms were faster than WT on D1 (Holm–Sidack posthoc test, $P < 0.001$, n = 46–105), but no difference was seen on D5.

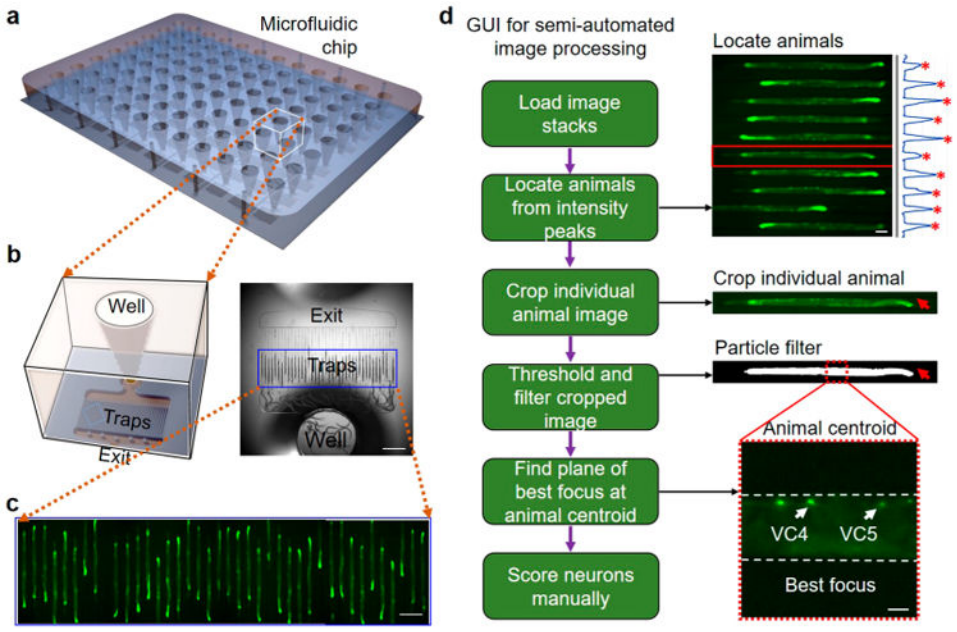

Figure 3.

High-content screening (HCS) platform for high-resolution imaging and high-content analysis of our APP model. (a) Overall illustration of the 96-well microfluidic chip for *C. elegans* HCS platform. (b) Magnified illustration (left) and an image (right) of a single well with 40 traps inside where multiple D3 adult *C. elegans* are immobilized. (c) Fluorescence images of SC_APP model animals immobilized within 40 traps. (d) Schematic of the graphic user interface (GUI) running several automated image-processing algorithms of the images and then displaying the best-focused image of the region of interest for allowing the user to perform a rapid phenotypic scoring. An example fluorescence image shows 10 channels with *C. elegans* and those which were automatically detected to have immobilized animals. The blue line profiles on the right present the projections of the intensities of each channel with peaks marked with red stars indicating that an immobilized animal is detected inside specific channels. The GUI then crops the images of channels with trapped animals and finds the animal body within these images by applying two algorithms; a thresholding algorithm that keeps 15% of the brightest pixels in the binary image, and a particle filtering algorithm based on the expected large size of the animal (see the second image with the red arrow showing the particle-filtered image). Once the animal body is identified, the GUI finds the best-focused image among the z-stacks and displays the magnified image of the centroid of each detected animal for manual scoring of the VC4 and 5 neurons. The bottom image shows the best focus at the animal's centroid where the subset of ventral cord (VC) cholinergic motor neurons of interest (VC4 and 5) are present and can rapidly be scored. White arrows mark VC4 and 5 neurons. Scale bars are 1 mm in (b), 200 μm in (c), and 100 and 20 μm in (d).

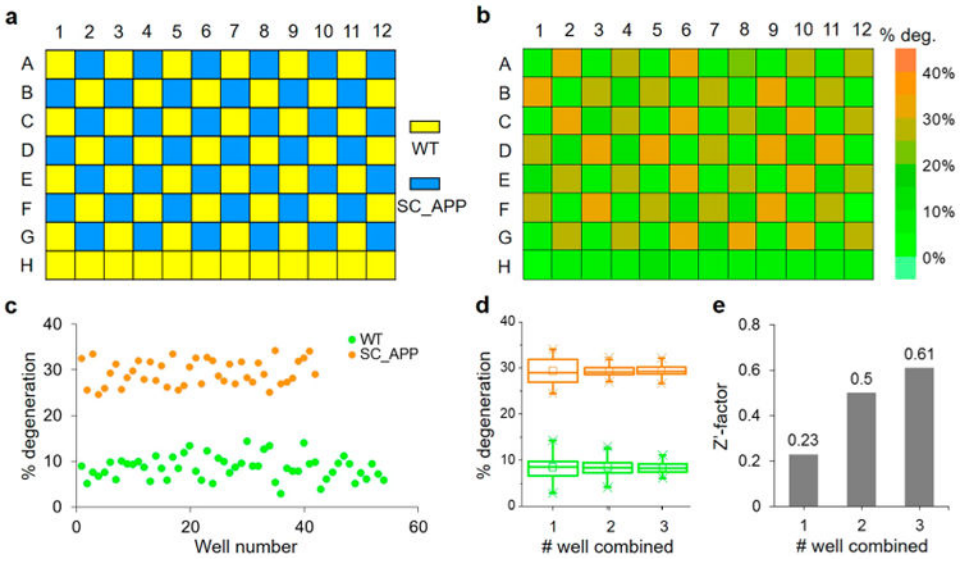

Figure 4.

Assay quality validation for the SC_APP animals imaged using the 96-well HCS chip and scored using the semiautomated image analysis program. (a) Checkered pattern for loading of the 96-well chip for characterization of the imaging platform performance using WT (yellow) and SC_APP (blue) model animals treated with 200 μM FUdR. (b) Degeneration rate map of individual wells. (c) Scatter plots of degeneration percentages of WT and SC_APP model animals for each well. (d) Box-chart plot of the degeneration percentages of WT (green) and SC_APP (orange) as calculated from 1, 2, and 3 consecutive wells. The line represents the median, the box represents the 25th and 75th percentiles of the data, and the stars denote the maximum and minimum values. (e) Z'-factor values plotted for all three conditions with 1, 2, and 3 consecutive wells pooled together.

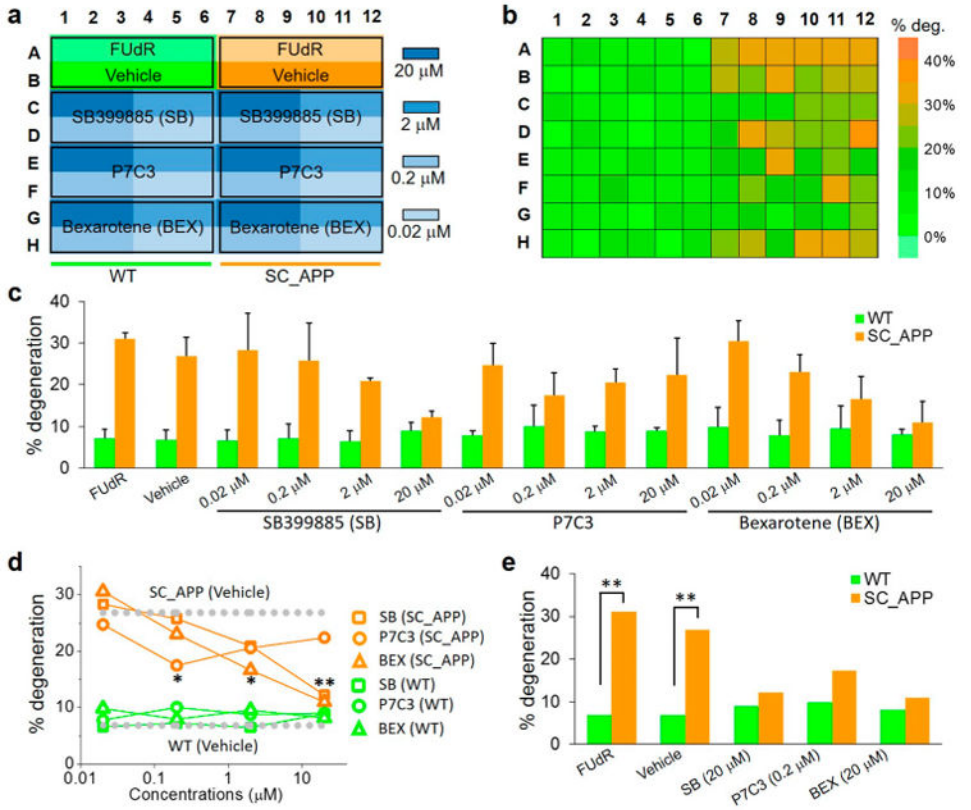

Figure 5.

Drug screening assay validation in the HCS platform for *C. elegans* SC_APP model. (a) Loading map of the chip with WT and SC_APP model animals with vehicle control (200 μM FUdR and 0.5% DMSO) and four doses (0.02, 0.2, 2, and 20 μM) of three drug compounds (SB, P7C3, and BEX). (b) Color map of average neuronal degeneration percentages for D3 animals. (c) Bar graph of degeneration percentages quantified from animal treatment with different chemicals at various concentrations. Data represented as mean + SD. (d) Dose dependence response of neuronal degeneration of animals. Control WT and SC_APP animals only treated with the vehicle are also represented by dotted lines. The stars indicate statistically significant degeneration rates of animals treated with chemical compounds with respect to those treated with controls. Each data point represents an average over three consecutive wells loaded with the same population of $n = 210$ neurons ($n = 105$ animals on average). The statistics were calculated using Fisher's exact test; $P < 0.001$ (**) and $0.001 < P < 0.01$ (*). (e) Degeneration percentages of WT (green) and SC_APP model (orange) animals treated with 200 μM FUdR, vehicle, and drugs at concentrations that showed the highest reductions in the degeneration rates. The statistics represent the comparison of degeneration rates between the SC_APP and WT animals treated with same chemical compounds.

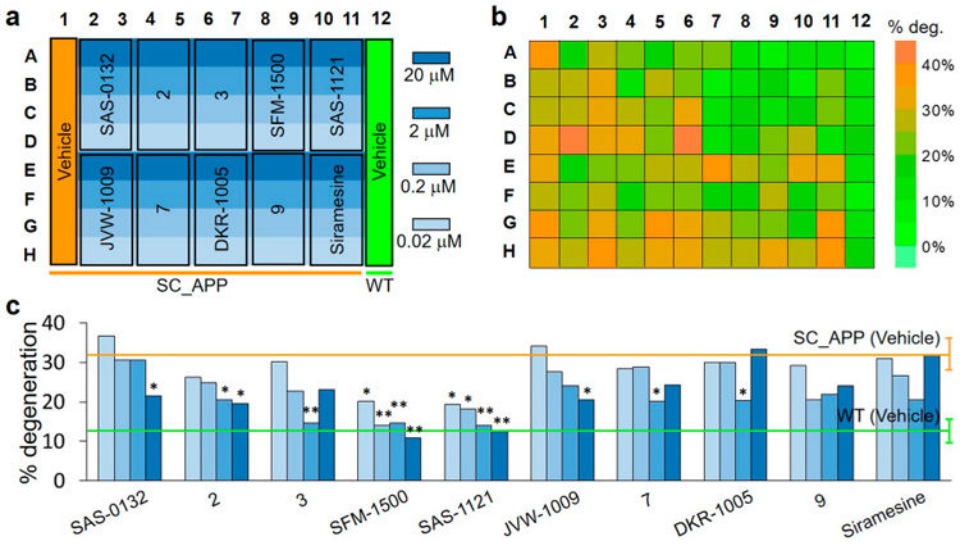

Figure 6.

Drug screening of novel compounds using the 96-well microfluidic chip on *C. elegans* SC_APP model. (a) Loading map of the chip with WT and SC_APP model animals with vehicle control (200 μM FUdR and 0.5% DMSO) and four doses (0.02, 0.2, 2, and 20 μM) for 10 different compounds. (b) Color map of average degeneration percentages of each individual well loaded with drug-treated D3 animals. (c) Dose-dependent neuronal degeneration percentages of treated animals. Green and orange lines represent the degeneration percentage (mean ± SD) of WT and SC_APP animals treated with vehicle only. The statistics were calculated using Fisher's exact test as compared to SC_APP animals treated with vehicle only; $P < 0.001$ (**) and $0.001 < P < 0.05$ (*); drug dose is indicated by the different shades of blue in panel (a).

Table 1
σ2R/Tmem97 Affinity of Norbenzomorphan Analogues

Compound	R1 [a]	R2 [a]	σ2R/Tmem97 K_i (nM)[b,c]	p-value
1 (SAS-0132)[d]	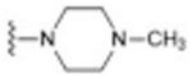	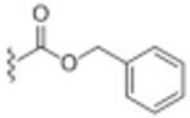	90 ± 19.8[e]	0.049
2	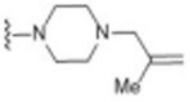	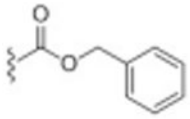	18 ± 3.5	0.054
3	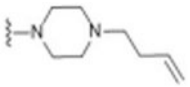	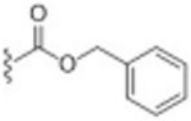	19 ± 4.2	<0.001
4 (SFM-1500)	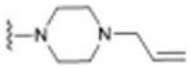	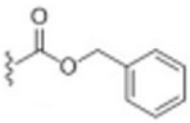	76 ± 28.8	<0.001
5 (SAS-1121)[d]	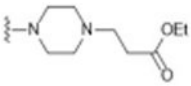	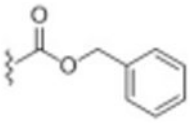	24 ± 10.3[e]	0.001
6 (JVW-1009)[d]	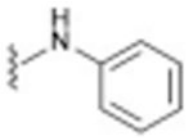	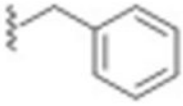	70 ± 8.5	0.031
7	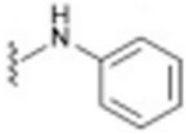		48 ± 21.7	0.027
8 (DKR-1005)[d]	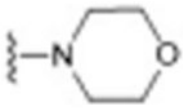	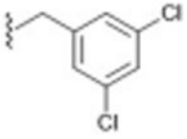	157 ± 84.9[e]	0.043

Compound	R1 [a]	R2 [a]	σ2R/Tmem97 K_i (nM)[b,c]	p-value
9	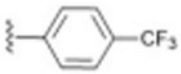	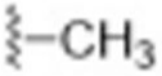	31 ± 9.10	0.058
Siramesine	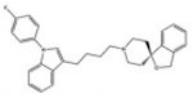		0.12[f]	0.079

[a] Basic structure for all compounds except siramesine is:

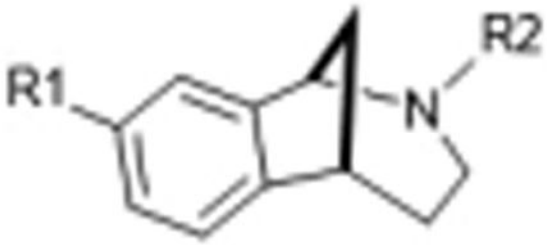

[b] K_i values reported as an average of two or more independent experiments.

[c] σ2R/Tmem97 sourced from rat PC12 cells.

[d] Compound previously published.[8,19,22]

[e] Differs from previously published values due to averaging of additional of K_i measurements.[8,22]

[f] Reference for siramesine K_i is ref 52.